Si Photonic Wire Waveguide Devices

Hirohito Yamada, *Member, IEEE*, Tao Chu, *Member, IEEE*, Satomi Ishida, and Yasuhiko Arakawa, *Senior Member, IEEE*

***Abstract*—Si photonic wire waveguides are attractive for constructing various optical devices that are extremely small because the waveguides can be bent with extremely small curvatures of less than a few micrometers of bending radius. We have fabricated optical directional couplers with the waveguides and demonstrated their fundamental characteristics. Their coupling length was extremely short, several micrometers, because of strong optical coupling between the waveguide cores. We have also demonstrated wavelength-demultiplexing functions for these devices with a long coupled waveguide. Optical outputs from a device with a 100-μm-long coupled waveguide changed reciprocally with a 20-nm wavelength spacing between the parallel and cross ports. We also demonstrated the operation of ultrasmall optical add-drop multiplexers (OADMs) with Bragg grating reflectors made up of the waveguides. The dropping wavelength bandwidth of the OADMs was less than 0.7 nm, and these dropping wavelengths could be precisely designed by adjusting the grating period. Using the Si photonic wire waveguide, we have also demonstrated thermo-optic switches. Metal thin-film heaters were evaporated onto the branch of a Mach–Zehnder interferometer that incorporated the waveguide to achieve switching operations by thermo-optic effects. In these switching operations, we observed more than 30 dB of extinction ratio, less than 90 mW of switching power, and less than 100 μs of switching speed.**

***Index Terms*—Integrated optics, lightwave circuit, optical add-drop multiplexer (OADM), optical directional coupler, optical interconnection, optical switch, optical waveguide, silicon-on-insulator (SOI), Si-wire thermo-optic effects.**

I. Introduction

SILICON photonics is receiving much interest because it enables the use of well-developed Si processing technologies as well as Si substrates that are cheaper than the compound semiconductor (GaAs or InP) substrates to fabricate a broad range of optical devices (light emitters, photodetectors, optical switches, optical passive components, and nonlinear optic devices) [1]–[4]. Furthermore, the Si photonics creates many possibilities such as photonic integration on Si substrates, monolithic integration of both electronic and photonic devices, and optical interconnection between electronic logic circuits on large-scale integrations. For the integration of photonics with a Si substrate, optical waveguides made up of Si and compact photonic devices that can be densely integrated on a Si substrate are essential. Thus far, Si-rib waveguides based on silicon-on-insulator (SOI) substrate have been studied for more than ten years [5], [6], and many optical components with waveguide structures have been demonstrated [1]. However, the Si-rib waveguide could not be bent to a small curvature because the bending losses became large when the bending radius was less than several hundred micrometers. Therefore, optical components constructed with the waveguides were not always compact. High-index contrast (high-Δ) optical waveguides are needed to achieve sharp bends in waveguides.

A search for the high-index contrast waveguide led us to the Si-channel waveguides [7]–[11] that consist of an Si core with an extremely small cross section and have a surrounding cladding of SiO_2 materials or air. Their basic characteristics have been investigated, and many functional devices have been demonstrated by using these waveguide structures such as channel-dropping filters with small ring waveguide resonators [10]–[12], lattice filters [13], optical switches [14], [15] or arrayed-waveguide gratings [16].

In this paper, we describe the characteristics of Si-channel waveguides with a nanoscale cross section that we therefore call "Si photonic wire waveguides." We will also describe various functional optical devices [directional couplers (DCs), wavelength demultiplexers (DEMUXs), optical add-drop multiplexers (OADMs), and optical switches] that we have developed based on this waveguide structure.

II. Si Photonic Wire Waveguide

The Si photonic wire waveguide is a channel waveguide consisting of a Si core with an extremely small cross section and a surrounding SiO_2 cladding material. Fig. 1(a) is a schematic of the waveguide structure. The cross-sectional Si-wire core is made as small as 300×300 nm in order to obtain a single-mode condition. The fabrication process is as follows. We used an SOI wafer with a 300-nm-thick single-crystal surface Si layer and a 1-μm-thick buried oxide (BOX) layer on a (100)Si substrate. First, we made a resist of the waveguide-core pattern on the surface Si layer by using electron-beam lithography. Next, with a resist mask, the surface Si layer was etched down to the BOX layer with an inductively coupled plasma (ICP) dry etcher, and this formed the Si-wire core. Finally, the Si-wire core that had been formed on the BOX layer was buried under a 1.0-μm-thick SiO_2 layer. Fig. 1(b) is a micrograph of a cross section of the waveguide. In this waveguide structure, we obtained an index

Manuscript received October 31, 2006; revised June 1, 2006. This work was supported in part by the New Energy and Industrial Technology Development Organization under the Photonic Network Project and in part by the Ministry of Education, Culture, Sports, Science, and Technology under the Focused Research and Development Project for the Realization of the World's Most Advanced IT Nation, IT Program.

H. Yamada is with the Fundamental and Environmental Research Laboratories, NEC Corporation, Ibaraki 305-8501, Japan, and also with the Optoelectronic Industry and Technology Development Association, Ibaraki 305-8501, Japan (e-mail: h-yamada@az.jp.nec.com).

T. Chu is with the Optoelectronic Industry and Technology Development Association, Ibaraki 305-8501, Japan (e-mail: tchu@frl.cl.nec.co.jp).

S. Ishida and Y. Arakawa are with the Nanoelectronics Collaborative Research Center, Institute of Industrial Science, University of Tokyo, Tokyo 153-8505, Japan, and also with the Research Center for Advanced Science and Technology, University of Tokyo, Tokyo 153-8505, Japan (e-mail: satomi@iis.u-tokyo.ac.jp; arakawa@iis.u-tokyo.ac.jp).

Digital Object Identifier 10.1109/JSTQE.2006.880611

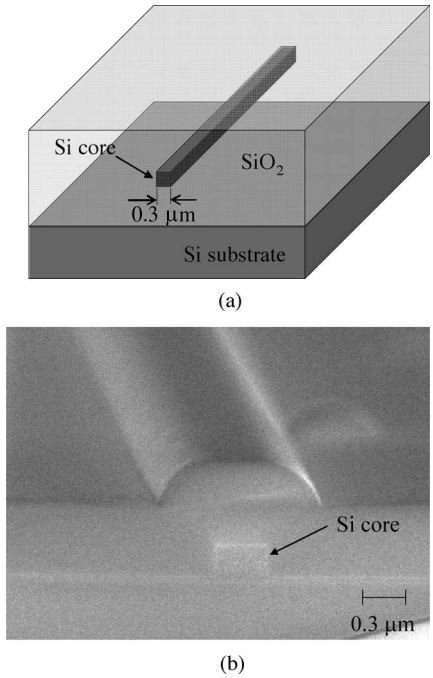

Fig. 1. Si photonic wire waveguide. (a) Structure. (b) Picture of the cross section.

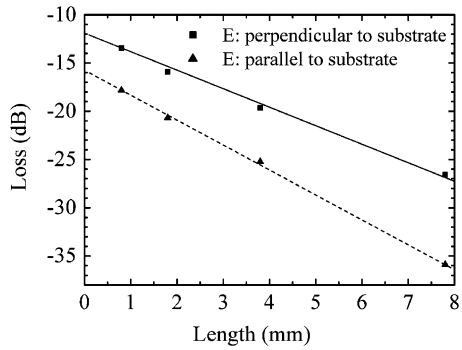

Fig. 2. Measured transmission losses for the Si photonic wire waveguides of various lengths.

contrast between the Si core and silica cladding (Δ) of 40%. Therefore, the strong optical confinement in the Si core makes it possible to bend the waveguide with a curvature of micrometer order.

First, we measured the propagation loss in the waveguide and also the coupling loss for a tapered single-mode fiber. The losses were measured using the cutback method, with tapered fibers optically coupled to both end facets of the waveguide, and introducing a light beam with 1.55-μm wavelength. Fig. 2 plots transmission losses measured for the Si photonic wire waveguides of various lengths. From the plot, we estimated the values of propagation loss and coupling loss, and found them to be 1.89 dB/mm and 6.1 dB/facet, respectively, when the polarization of the electric field vector was perpendicular to the substrate. The corresponding losses for the other polarization (i.e., the electric field vector parallel to the substrate) were a little higher than these values; they were 2.56 dB/mm and 8 dB/facet,

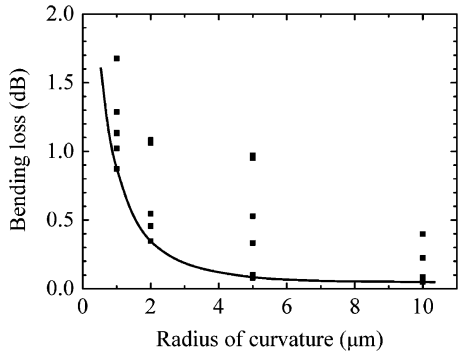

Fig. 3. Measured bending losses for the Si photonic wire waveguides with right-angled bends of various curvatures.

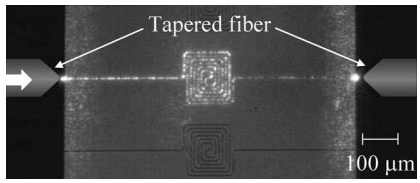

Fig. 4. Infrared image from the top of a coil pattern of the waveguide when propagating the light beam.

respectively. We think the higher propagation loss for the polarization electric field parallel to the substrate was caused by sidewall roughness of the waveguide, and we can further reduce both propagation losses by introducing a sidewall smoothing process with thermal oxidation [11]. The propagation loss and coupling loss were almost constant in the measured wavelength range of 1510–1640 nm.

Next, we measured the bending losses of the waveguides. We fabricated various waveguides with various numbers and curvatures of right-angle bends. Fig. 3 plots bending losses measured for the waveguides with various curvatures of right-angle bend. In this case, we measured only for the polarization electric field perpendicular to the substrate. The bending loss increased with reducing bending radius, and it was practically zero when the bending radius of the waveguide was larger than 5 μm. Fig. 4 is an infrared image from the top of the coil pattern of the waveguide when a light beam was propagated through it. The coil pattern includes 28 right-angle bends with a bending curvature of 10 μm. We clearly observed the light output from the end facet, and this shows that the bending loss of the waveguide was small.

A beam spot-size converter can improve the coupling loss between the waveguides and the optical fibers and this has also been investigated. Such a converter for the Si photonic wire waveguide with a tapered core and a polymer cladding structure was previously demonstrated and reported [17]. Less than 1 dB of low coupling loss for a thermal-diffusion expanded core fiber was achieved with the converter.

We employed a very simple structure with only a tapered core as shown in Fig. 5(a). The length of the tapered core was 200 μm and its tip width was 100 nm. Fig. 5(b) represents the measured transmission loss spectra for a total 1.63-mm-long waveguide with beam spot-size converters for both end facets.

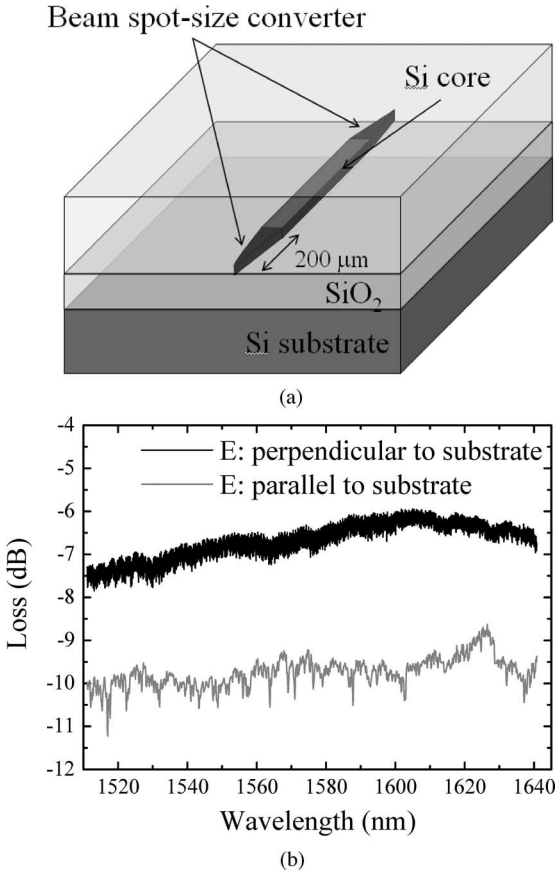

Fig. 5. 1.63-mm-long waveguide with spot-size converter. (a) Structure. (b) Transmission loss spectra.

The total losses of the waveguide including coupling losses to tapered fibers were about 7 dB for the polarization electric field perpendicular to the substrate and about 10 dB for the other polarization (electric field parallel to the substrate) at a wavelength of around 1.55 μm. Therefore, we estimated the coupling losses per facet to be 2.0 dB and 2.9 dB, respectively, for the two polarizations with these measured loss values and previously described propagation loss values per unit length of the waveguide.

Although the spot-size converter is simple and effective for reducing coupling loss, further study is needed regarding control of the tip position because the coupling loss strongly depends on the distance between the end facet and the tip position of the tapered core. Therefore, some method should be developed for truing up the tip position to the end facet.

III. Optical DCs

In optical interconnections, waveguide junctions or branches are essential. Optical DCs can be used for the waveguide branches, and they also work as power combiner/dividers with arbitrary power dividing ratio. Furthermore, they are also the most fundamental elements for constructing various optical devices. They are used to construct power combiners/dividers, wavelength multiplexers (MUXs)/DEMUXs, add-drop multiplexers, and optical switches. In Section III, we describe optical DCs based on Si photonic wire waveguides and discuss their characteristics.

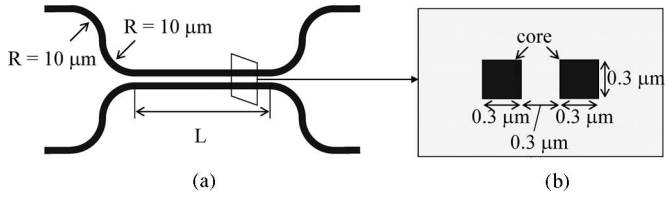

Fig. 6. Coupled waveguide portion of DC. (a) Top-view structure. (b) Cross section.

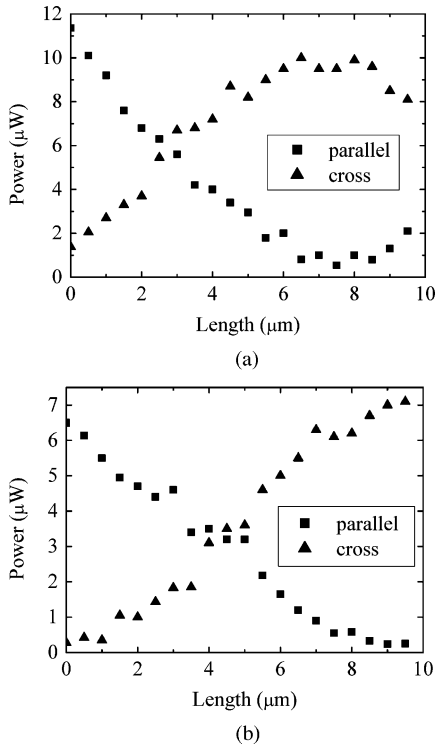

Fig. 7. Measured light output powers from both the output ports of the DCs with various coupled waveguide lengths from 0 to 10 μm. (a) Electric field perpendicular to the substrate. (b) Electric field parallel to the substrate.

Fig. 6 presents the top and cross-sectional views of the coupled waveguide portion of the DC. The Si cores had 0.3-μm^2 cross sections and were 0.3 μm apart at the coupled waveguide portion. The S-shaped waveguides were connected to both the input and output ports of the coupled waveguides to separate the light beam delivered to the two waveguide cores and to separate it again as it excited the waveguide cores. The radius of curvature for the S-shaped waveguide was 10 μm, so the overall lengths of the DCs were 40 μm longer than the lengths of coupled waveguides. We fabricated various lengths of the DC samples with different coupled waveguide lengths L.

The light output power from both output ports of the DCs was measured when a 1.55-μm-wavelength laser beam was directed into one of the input ports. The output powers measured for DCs with various coupled waveguide lengths from 0 to 10 μm are plotted in Fig. 7. As the characteristics depend on the polarization, we measured the output powers for both the polarizations.

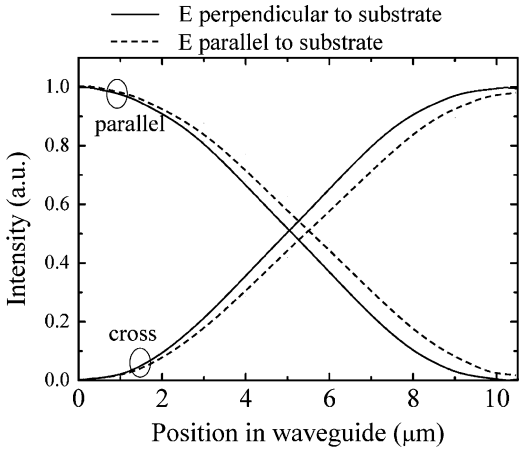

Fig. 8. Calculated optical intensity in the cores of the coupled waveguide plotted against their positions in the waveguide.

In the figure, "parallel" and "cross" mean the plots of optical powers from the same and different waveguide cores, respectively, as the lightwave was launched. The powers from both the output ports were complementary, and for both the polarizations they changed sinusoidally according to the coupled waveguide length. Although the values measured for $L = 0$ do not correspond to an actual coupled waveguide length of zero (because the S-shaped waveguides at the entrance sections act as part of the coupled waveguide), the coupling length was estimated to be about 10 μm for polarization of the electric field perpendicular to the substrate and to be 11 μm for polarization of the electric field parallel to the substrate. The coupling from the S-shaped waveguides was estimated by extrapolation to correspond to a coupling length L of 2 μm.

We also calculated the characteristics of the coupled waveguide by using a three-dimensional (3-D) finite-difference time-domain method. Fig. 8 is a plot of the optical intensity in the core of the waveguides. In this figure, the respective solid and broken lines describe the plots for polarizations of electric field perpendicular and parallel to the substrate. The coupling length was about 10 μm when the polarization of the electric field was perpendicular to the substrate, and it was found to be a little longer (11 μm) when the electric field was parallel to the substrate. These results were in good agreement with the experimental results.

We also fabricated DCs with longer coupled waveguides. Fig. 9(a) plots the wavelength dependence of transmittance measured for the two output ports (parallel and cross) of a DC with a 100-μm-long coupled waveguide. We found a strong dependence on the wavelength: at 1549 nm, most of the light power was output from the parallel port, and at 1569 nm, most of the light power was output from the cross port. The extinction ratio was greater than 20 dB, and the insertion loss around 1550 nm was about 15 dB. We think that most of the loss was the coupling loss of the tapered fibers (6.1 dB $\times 2$ for both facets) and the rest was propagation loss. The wavelength dependence of the calculated light output power [Fig. 9(b)] was similar to that observed in the measured light output power. We also measured for DCs with longer coupled waveguides ($L = 800$ μm). The

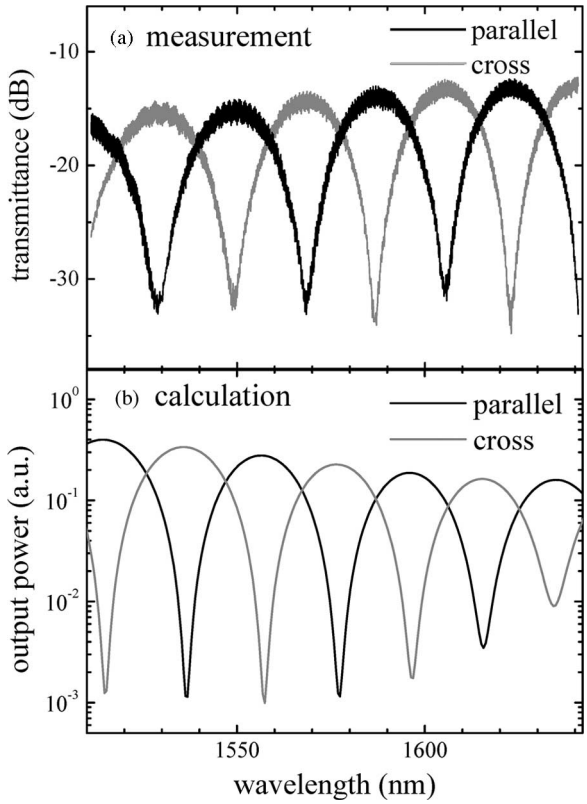

Fig. 9. Wavelength dependence of the light outputs from a 100-μm-long DC. (a) Measured transmission losses. (b) Calculated light output powers.

optical output powers from the parallel and cross ports of an 800-μm-long device changed reciprocally with a 2.5-nm wavelength periodicity [18].

IV. OADM

Wavelength MUXs/DEMUXs are key devices for wavelength-division multiplexing (WDM) in photonic networks. Many types of wavelength MUX/DEMUX devices have been studied. Examples are a ring-resonator channel-dropping filter (CDF) [10]–[12], a lattice-filter CDF [13], and OADMs with a Bragg-grating reflector composed of a Mach–Zehnder interferometer (MZI) [19] or a directional coupler [20]. Among these, the Bragg-reflector OADMs are promising for wavelength MUX/DEMUX because of their flat-topped bandpass spectra and wide free spectral ranges as well as their flexible wavelength selectivity. In Section IV, we describe an ultrasmall Bragg-reflector OADM based on Si photonic wire waveguides.

As illustrated in Fig. 10, the OADMs we made were composed of two Si photonic wire straight waveguides with Bragg gratings and two 3-dB couplers based on Si photonic wire waveguide DCs. The 3-dB coupler was about 5-μm long because the effective coupling length of the DC was about 10 μm when the distance between the waveguide cores was 300 nm [18]. The Bragg gratings were formed by making small fins on the sidewall of the straight waveguides as shown in the figure. The projections of the fins were 10 nm, and the grating was

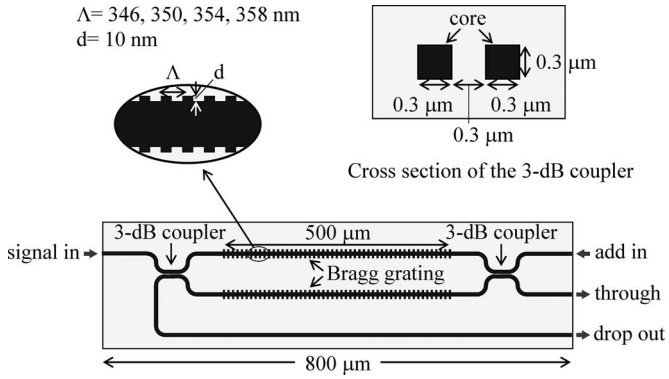

Fig. 10. Structure of the OADM based on the Si photonic wire waveguide.

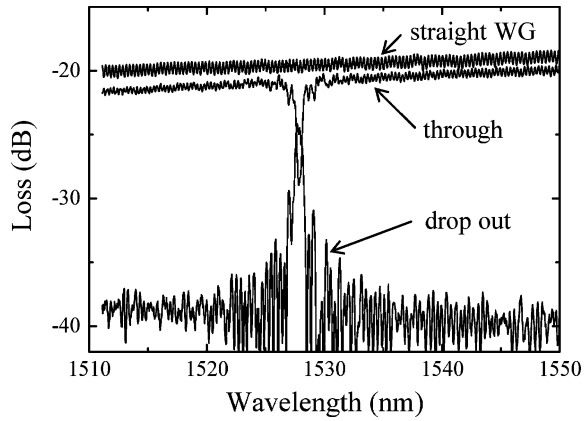

Fig. 11. Transmission loss spectra of the OADM and the straight waveguide.

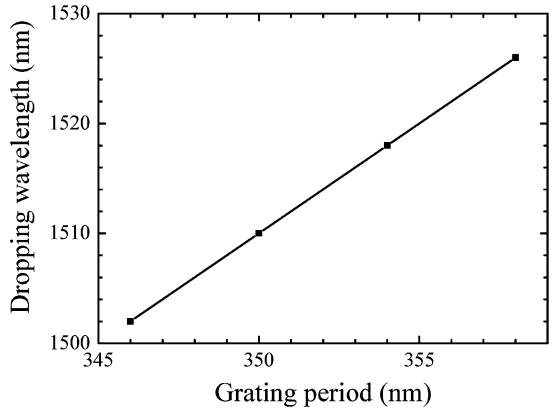

Fig. 12. Relation between the dropping wavelength and the grating period.

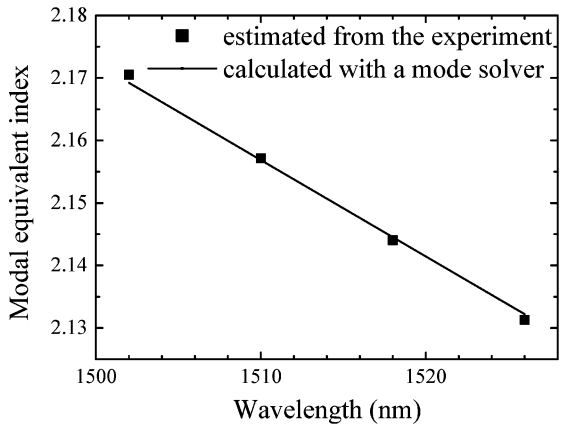

Fig. 13. Relation between the wavelength and the modal equivalent index calculated with a mode solver (*lines*) and estimated experimentally (*squares*).

500-μm long. We tested four types of gratings with periods Λ of 346-, 350-, 354-, and 358 nm. We connected S-shaped waveguides with a 10-μm radius to both the input and output ports of the 3-dB couplers to separate the light output from the two waveguide cores of the 3-dB coupler. The net length of the OADM devices was about 600 μm. For measurement, the devices were cut from the wafer in a sample bar that included many of these devices. The total length of the devices used for the measurement, including the simple straight waveguides bringing light to the devices, was about 800 μm [21].

The characteristics were measured with tapered optical fibers coupled to the input and output ports of the OADMs. Because the measurement depends on the polarization of the electric field, we controlled the polarization of the incident light beam by keeping the electric field perpendicular to the substrate. Fig. 11 plots the transmission loss spectra for the through port and drop-out port of the OADMs. The dropping center wavelength was about 1527 nm when the grating period was 358 nm, and the 3-dB bandwidth was 0.7 nm. The extinction ratio for the through output at the dropping wavelength was about 8 dB. The extinction ratio can be improved by increasing the reflectivity of the Bragg grating by increasing the height of its fins. The insertion loss was 22 dB for the through port and 24 dB for the drop-out port. The 2-dB difference in the through port and drop-out port losses is because the output waveguide for the drop-out port was about 700 μm longer than that for the through port. The loss spectrum measured for a simple straight waveguide with the same length as the OADM is also given in Fig. 11. From a comparison of the measured loss values between the straight waveguide and the OADM, we can estimate the excess loss caused by the device structures to be less than 2 dB. We have not yet designed the device to have characteristics independent of polarization; hence, for the other polarization (electric field parallel to the substrate), we observed a broad dip in the transmission spectrum for the through port at a wavelength that was about 20 nm longer than the drop wavelength for the primary polarization (electric field perpendicular to the substrate).

The relation between the grating period and the dropping wavelength is shown in Fig. 12. The dropping wavelength increased with increase in the grating period. The relation between the dropping wavelength (λ) and the grating period (Λ) is described by

$$\lambda = 2n_{\mathrm{eq}}\Lambda. \tag{1}$$

Here, n_{eq} is the modal equivalent index of the propagating lightwave in the Si photonic wire waveguide. We estimated the values of n_{eq} with this equation, and plotted them against the wavelength (Fig. 13). In this wavelength range, the estimated n_{eq} values decreased with increasing wavelength.

Also shown in the figure is a line indicating n_{eq} values. We calculated these values using a mode solver tool assuming the refractive indices of the Si core and silica cladding are 3.5 and 1.46, respectively. This calculated line is in good agreement with the n_{eq} values estimated from the measurement. We can therefore use this relation between n_{eq} and the wavelength to precisely design the dropping wavelengths of the devices, although we need to control the device temperature precisely because a 6-K temperature change causes the dropping wavelength to shift by 0.7 nm.

V. Thermo-Optic Switch

Optical switches are also key devices for nodes in photonic networks. So far, a lot of research has been devoted to optical switches [14], [15], [22]–[24] and/or optical modulators [25], [26] fabricated on SOI substrates. However, the device sizes for the MZI-type optical switches [14], [15], [22]–[24] and/or optical modulators [25] were not always small enough for integration. However, the ring-resonator-type optical switches (modulators) [26] were very small. Also, the wavelength of the switched optical signal must be fixed, which means the switching bandwidth is very narrow. Therefore, from the application point of view, the ring-resonator type optical switch is difficult to use. In Section V, we describe very compact MZI-type optical switches based on Si photonic wire waveguides and discuss their characteristics.

We fabricated the MZI-type 1×1 and 1×2 optical switches. Microscopic views of the switches are shown in Fig. 14(a) and (b), respectively. The 1×1 and 1×2 switches were composed of a Y-splitter for dividing the input light beam, a thermo-optically controlled MZI for tuning the phase of the propagating light beam, and a 3-dB coupler with a Y-splitter for the 1×1 switch or with a DC for the 1×2 switch [27]. All of them were based on Si photonic wire waveguides on an SOI substrate. The cross section of the Si photonic wire waveguides was 300×300 nm. The coupled waveguide length of the DC for the 3-dB couplers was 5 μm, and the length of the MZI branches was 40 μm. Metal thin-film heaters were evaporated on the top silica cladding layer just above the MZI branches for providing thermo-optical control. It should be noted that the metal heaters were formed on both the MZI branches to provide a structural symmetry between them, but only one of the two heaters on the two MZI branches was connected to the electrode pads, while the other one was only a dummy heater. The electric resistance of the active heater was $30\,\Omega$ for the 1×1 switch and $100\,\Omega$ for the 1×2 switch. Excluding the electrode pads, the net device footprints were 140×65 μm for the 1×1 switch and 85×30 μm for the 1×2 switch, respectively. The 1×2 switch was more compact than the 1×1 switch because the design of the Y-splitter used in the 1×2 switch was optimized, compared with that used in the 1×1 switch. The optical switches were characterized by the tapered fibers used for coupling light in the devices. To measure the response speed of the switch, we also used a pulse power supply.

First, we characterized the 1×1 switch. At 1550 nm, we measured the transmission loss while changing the heating power,

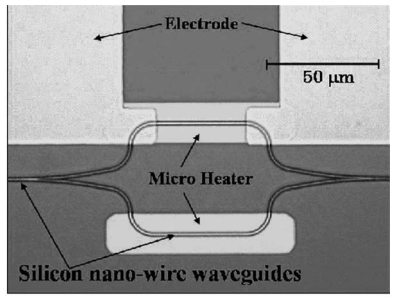

(a)

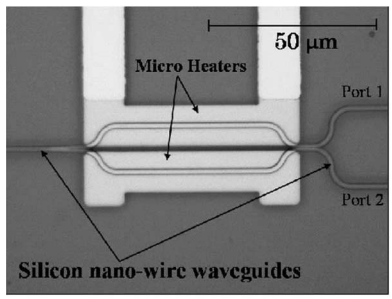

(b)

Fig. 14. Thermo-optic switch based on the Si photonic wire waveguides. (a) 1×1 switch. (b) 1×2 switch.

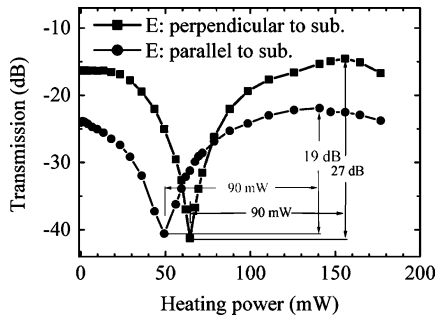

Fig. 15. Transmission loss of the 1×1 switch as a function of the heating power.

as plotted in Fig. 15. We measured it for both the polarizations of the incident lightbeam: the electric field vector perpendicular and parallel to the substrate. As shown in Fig. 15, the maximum and minimum transmissions did not appear at the same heating power for both the polarizations due to the polarization-dependent propagation constant of the waveguide. This polarization dependence might be reduced by using properly controlled stress-induced birefringence with silica cladding, as is done for the Si-rib waveguides [28]. The maximum transmittance in Fig. 15 shows a device insertion loss of 15 dB for the polarization electric field perpendicular to the substrate and 22 dB for the polarization electric field parallel to the substrate. The insertion losses were mainly caused by the propagation losses and the coupling losses between the fibers and the waveguides. They were about 2 dB/mm and 6 dB/facet for the polarization electric field perpendicular to the substrate and about 2.5 dB/mm and 8 dB/facet for the polarization electric field parallel to the substrate as mentioned earlier. The obtained maximum extinction ratio for the 1×1 switch was 27 dB for the polarization electric

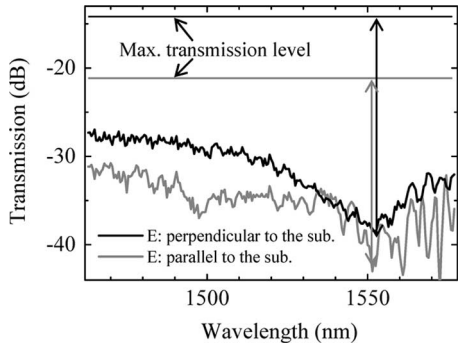

Fig. 16. Wavelength detuning characteristics of transmission loss for the 1×1 switch.

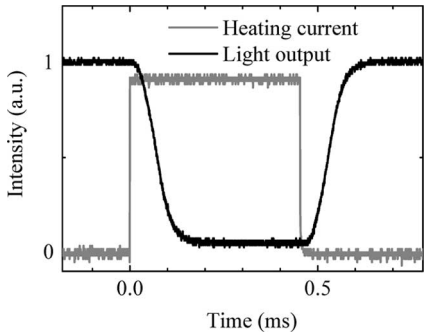

Fig. 17. Light output waveform response to a heating current pulse.

field perpendicular to the substrate and 19 dB for the polarization electric field parallel to the substrate. The heating power needed for complete switching was approximately 90 mW, and this value was the same for both the polarizations. Although this 90-mW switching power is still high for integration, it can be decreased by optimizing the device structure [22], [23].

We investigated the wavelength–detuning characteristics of the 1×1 switch by tuning the wavelength of the incident light beam while fixing the heating power at the maximum extinction point for both the polarizations at 1550-nm wavelength. The characteristics are presented in Fig. 16. As the figure shows, we found that the wavelength can be detuned by over 15 nm for both polarizations while maintaining an extinction ratio of more than 20 dB for the polarization electric field perpendicular to the substrate and 15 dB for the polarization electric field parallel to the substrate. This means the switching bandwidth is more than 15 nm under the operating conditions described earlier.

The switching response time was measured at 1550-nm wavelength. As plotted in Fig. 17, we found that the switching ON/OFF time was typically around $100\ \mu$s. However, further improving the speed of the thermally controlled MZI switch to less than $10\ \mu$s might be possible by reducing the thickness of the lower silica cladding layers [22], [23], although using a cladding layer that is too thin might increase the propagation loss.

Next, we measured the dependence of the transmittance of the 1×2 switch at 1550 nm on the heating power. Due to the polarization dependence of the device, we only conducted the measurement for the polarization electric field perpendicular to

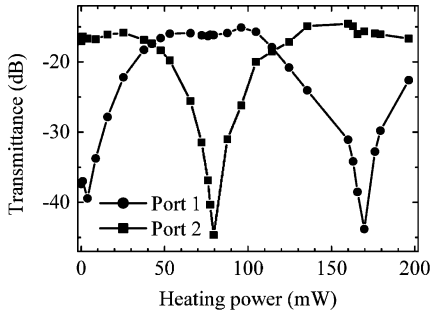

Fig. 18. Transmission loss of the 1×2 switch as a function of the heating power.

the substrate. As can be seen in Fig. 18, as the heating power was increased, the light outputs from both the ports (1 and 2) alternately switched ON and OFF. The light output from port 2 was minimal at 80 mW, while that from port 1 was minimal at 170 mW. Therefore, the switching power needed to change output ports was 90 mW. The device insertion loss was about 15 dB, and the maximum extinction ratio obtained was more than 30 dB. The switching response time and wavelength-detuning characteristics of the 1×2 switch should be similar to those of the 1×1 switch since the fundamental structures of the devices are similar.

VI. Summary

We have described the Si photonic wire waveguides and ultrasmall optical devices fabricated with this waveguide structure. We have reported our measurements of propagation loss and bending losses for the waveguides. The bending loss was practically negligible when the bending radius of the waveguide was larger than 5 μm. We also fabricated optical DCs with the waveguides and evaluated their fundamental characteristics. We found that they had extremely short coupling lengths, typically about 10 μm, which means that they can be used as compact optical power dividers or combiners. We also demonstrated wavelength-selective characteristics of light output from long DCs. The optical outputs from the parallel and cross ports of a 100-μm-long device changed reciprocally with a 20-nm wavelength periodicity, and this indicates that this device could be used as a wavelength MUX/DEMUX.

We have also demonstrated ultrasmall OADMs with waveguides having Bragg grating reflectors. We found that the devices have the potential of providing a dropping wavelength resolution of less than 0.8 nm that satisfies the requirements for dense WDM systems with 100-GHz channel spacing. We also found that the dropping wavelength can be designed precisely by adjusting the grating period.

Furthermore, using the waveguide, we have also demonstrated the operation of very compact thermo-optic switches. Metal thin-film heaters were evaporated on the branch of a Mach–Zehnder interferometer that incorporated the waveguide to accomplish switching operations by thermo-optic effects. In these switching operations, we observed more than 30 dB of extinction ratio, less than 90 mW of switching power and less

than 100 μs of switching speed with footprints smaller than $100 \times 50\,\mu\mathrm{m}^2$ for the optical switches.

Therefore, we conclude that the Si photonic wire waveguides are attractive platforms for constructing various optical devices that are extremely small. We believe that large-scale optical-integrated circuits incorporating Si photonic wire waveguide devices will be in practical use in the near future.

ACKNOWLEDGMENT

The authors would like to thank M. Tokushima, A. Gomyo, J. Ushida, M. Shirane, and S. Nakamura for their useful discussions and K. Ohashi and J. Sone for their encouragement.

REFERENCES

[1] B. Jalali, S. Yegnanarayanan, T. Yoon, T. Yoshimoto, I. Rendina, and F. Coppinger, "Advances in silicon-on-insulator optoelectronics," *IEEE J. Sel. Topics Quantum Electron.*, vol. 4, no. 6, pp. 938–947, Nov.–Dec. 1998.

[2] L. C. Kimerling, "Silicon microphotonics," *Appl. Surf. Sci.*, vol. 159–160, pp. 8–13, 2000.

[3] L. Pavesi, "Will silicon be the photonic material of the third millennium?," *J. Phys., Condens. Matter*, vol. 15, pp. R1169–R1196, 2003.

[4] G. T. Reed, "The optical age of silicon," *Nature*, vol. 427, pp. 595–596, 2004.

[5] R. A. Soref, J. Schmidtchen, and K. Petermann, "Large single-mode rib waveguides in GeSi–Si and Si-on-SiO_2," *IEEE J. Quantum Electron.*, vol. 27, no. 8, pp. 1971–1974, Aug. 1991.

[6] A. G. Rickman, G. T. Reed, and F. Namavar, "Silicon-on-insulator optical rib waveguide loss and mode characteristics," *J. Lightw. Technol.*, vol. 12, no. 10, pp. 1771–1776, Oct. 1994.

[7] C. Manolatou, S. G. Johnson, S. Fan, P. R. Villeneuve, H. A. Haus, and J. D. Joannopoulos, "High-density integrated optics," *J. Lightw. Technol.*, vol. 17, no. 9, pp. 1682–1692, Sep. 1999.

[8] A. Sakai, G. Hara, and T. Baba, "Propagation characteristics of ultrahigh-Δ optical waveguide on silicon-on-insulator substrate," *Jpn. J. Appl. Phys.*, vol. 40, pp. L383–L385, 2001.

[9] Y. A. Vlasov and S. J. McNab, "Losses in single-mode silicon-on-insulator strip waveguides and bends," *Opt. Express*, vol. 12, pp. 1622–1631, 2004.

[10] P. Dumon, W. Bogaerts, V. Wiaux, J. Wouters, S. Beckx, J. V. Campenhout, D. Taillaert, B. Luyssaert, P. Bienstman, D. V. Thourhout, and R. Baets, "Low-loss SOI photonic wires and ring resonators fabricated with deep UV lithography," *IEEE Photon. Technol. Lett.*, vol. 16, no. 5, pp. 1328–1330, May 2004.

[11] T. Tsuchizawa, K. Yamada, H. Fukuda, T. Watanabe, J. Takahashi, M. Takahashi, T. Shoji, E. Tamachika, S. Itabashi, and H. Morita, "Microphotonics devices based on silicon microfabrication technology," *IEEE J. Sel. Topics Quantum Electron.*, vol. 11, no. 1, pp. 232–240, Jan.–Feb. 2005.

[12] B. E. Little, J. S. Foresi, G. Steinmeyer, E. R. Thoen, S. T. Chu, H. A. Haus, E. P. Ippen, L. C. Kimerling, and W. Greene, "Ultra-compact Si–SiO_2 microring resonator optical channel dropping filters," *IEEE Photon. Technol. Lett.*, vol. 10, no. 4, pp. 549–551, Apr. 1989.

[13] K. Yamada, T. Shoji, T. Tsuchizawa, T. Watanabe, J. Takahashi, and S. Itabashi, "Silicon-wire-based ultrasmall lattice filters with wide free spectral ranges," *Opt. Lett.*, vol. 28, pp. 1663–1664, 2003.

[14] R. L. Espinola, M.-C. Tsai, J. T. Yardley, and R. M. Osgood, Jr., "Fast and low-power thermooptic switch on thin silicon-on-insulator," *IEEE Photon. Technol. Lett.*, vol. 15, no. 10, pp. 1366–1368, Oct. 2003.

[15] M. W. Geis, S. J. Spector, R. C. Williamson, and T. M. Lyszczarz, "Submicrosecond submilliwatt silicon-on-insulator thermooptic switch," *IEEE Photon. Technol. Lett.*, vol. 16, no. 11, pp. 2514–2516, Nov. 2004.

[16] T. Fukazawa, F. Ohno, and T. Baba, "Very compact arrayed-waveguide-grating demultiplexer using Si photonic wire waveguides," *Jpn. J. Appl. Phys.*, vol. 43, pp. L673–L675, 2004.

[17] T. Shoji, T. Tsuchizawa, T. Watanabe, K. Yamada, and H. Morita, "Low loss mode size converter from 0.3 μm square Si wire waveguides to singlemode fibers," *Electron. Lett.*, vol. 38, no. 25, pp. 1669–1670, Dec. 2002.

[18] H. Yamada, T. Chu, S. Ishida, and Y. Arakawa, "Optical directional coupler based on Si-wire waveguides," *IEEE Photon. Technol. Lett.*, vol. 17, no. 3, pp. 585–587, Mar. 2005.

[19] G. E. Kohnke, C. H. Henry, E. J. Laskowski, M. A. Cappuzzo, T. A. Strasser, and A. E. White, "Silica based Mach–Zehnder add-drop filter fabricated with UV induced gratings," *Electron. Lett.*, vol. 32, no. 17, pp. 1579–1580, Aug. 1996.

[20] N. Ofusa, T. Saito, T. Shimoda, T. Hanada, Y. Urino, and M. Kitamura, "An optical add-drop multiplexer with a grating-loaded directional coupler in silica waveguides," *IEICE Trans. Electron.*, vol. E82-C, pp. 1514–1517, 1999.

[21] H. Yamada, T. Chu, S. Ishida, and Y. Arakawa, "Optical add-drop multiplexers based on Si-wire waveguides," *Appl. Phys. Lett.*, vol. 86, p. 191107, 2005.

[22] G. V. Treyz, "Silicon Mach–Zehnder waveguide interferometers operating at 1.3 μm," *Electron. Lett.*, vol. 27, no. 2, pp. 118–120, Jan. 1991.

[23] U. Fischer, T. Zinke, B. Schuppert, and K. Petermann, "Singlemode optical switches based on SOI waveguides with large cross-section," *Electron. Lett.*, vol. 30, no. 5, pp. 406–408, Mar. 1994.

[24] M. Harjanne, M. Kapulainen, T. Aalto, and P. Heimala, "Sub-μs switching time in silicon-on-insulator Mach–Zehnder thermooptic switch," *IEEE Photon. Technol. Lett.*, vol. 16, no. 9, pp. 2039–2041, Sep. 2004.

[25] A. Liu, R. Jones, L. Liao, D. Samara-Rubio, D. Rubin, O. Cohen, R. Nicolaescu, and M. Paniccia, "A high-speed silicon optical modulator based on a metal-oxide-semiconductor capacitor," *Nature*, vol. 427, pp. 615–617, 2004.

[26] Q. Xu, B. Schmidt, S. Pradhan, and M. Lipson, "Micrometer-scale silicon electro-optic modulator," *Nature*, vol. 435, pp. 325–327, 2005.

[27] T. Chu, H. Yamada, S. Ishida, and Y. Arakawa, "Compact $1 \times N$ thermo-optic switches based on silicon photonic wire waveguides," *Opt. Express*, vol. 13, pp. 10109–10114, 2005.

[28] S. P. Chan, C. E. Png, S. T. Lim, G. T. Reed, and V. M. N. Passaro, "Single mode, polarization independent waveguides in silicon-on-insulator," presented at the IEEE/LEOS 1st Int. Conf. Group IV Photon., ThP21, Hong Kong, Sep. 29–Oct. 1, 2004.

Hirohito Yamada (A'04–M'04) received the B.E. degree from Kanazawa University, Kanazawa, Japan, in 1981, and the M.E. and the Ph.D. degrees from Tohoku University, Sendai, Japan, in 1983 and 1987, respectively, all in electronics engineering.

In 1987, he joined the Opto-Electronics Research Laboratories, NEC Corporation, Ibaraki, Japan, where he was engaged in research on semiconductor lasers for optical communications. From 1991 to 1997, he was with the NEC Kansai Electronics Research Laboratory, Kyoto, Japan, where he was engaged in research on semiconductor lasers for optical subscriber network systems. From 1998, he was with NEC Tsukuba Research Laboratory, Ibaraki, where he was engaged in research on nanophotonic devices for photonic crystals. He is currently a Principal Researcher at the Fundamental and Environmental Research Laboratories, NEC Corporation, Ibaraki.

Dr. Yamada is a Member of the Institute of Electronics, Information, and Communication Engineers and the Japan Society of Applied Physics.

Tao Chu (M'04) received the B.S. degree in electronics and information engineering from Sichuan University, Chengdu, China, in 1991, and the M.Eng. degree in electronics and information science and the Dr.Eng. degree in information and production science from Kyoto Institute of Technology, Kyoto, Japan, in 1999 and 2002, respectively.

From 1991 to 1995, he was a Research Associate at the East-China Microelectronic Research Institute, Hefei, China. From 2001 to 2003, he was a Japan Society for the Promotion of Science Fellow at the Kyoto Institute of Technology, Kyoto. Since 2003, he has been a Researcher at the Optoelectronic Industry and Technology Development Association, Tsukuba, Japan. His current research interests include optical communication devices and optical integration based on silicon nanophotonics.

Satomi Ishida was born in Kyoto, Japan, in 1965. He received the B.Sc. degree from Shinsyu University, Nagano, Japan, in 1988.

From 1988 to 1993, he was with Murata Manufacturing Company, Ltd. In 1993, he was transferred as a Technical Associate at the Nanoelectronics Collaborative Research Center, Institute of Industrial Science, University of Tokyo, Tokyo, Japan. Since then, he has been engaged in research on the fabrication technology of quantum structures for semiconductor lasers in fiber optical communication systems. In 1997, he was a Research Associate at the Institute of Industrial Science, University of Tokyo. He is currently a Research Associate at the Research Center for Advanced Science and Technology, University of Tokyo. His current research interests include nanofabrication processes based on electron-beam lithography and wet/dry etching techniques.

Yasuhiko Arakawa (S'77–M'80–SM'04) received the B.S., M.S., and Ph.D. degrees from the University of Tokyo, Tokyo, Japan, in 1975, 1977, and 1980, respectively, all in electrical engineering.

He joined the University of Tokyo as an Assistant Professor in 1980, and was a Full Professor in 1993. He is currently a Professor at the Research Center for Advanced Science and Technology, University of Tokyo. He is a Project Leader at the Ministry of Education, Culture, Sports, Science, and Technology and the Ministry of Economy, Trade, and Industry projects on nanophotonic devices. He is also the Director of Nanoelectronics Collaborative Research Center, Institute of Industrial Science, University of Tokyo. His current research interests include growth and physics of semiconductor nanotechnologies for optoelectronic device applications such as quantum dot lasers, single photon emitters, and future quantum information devices.

Dr. Arakawa has been a General Chair for the 1998 IEEE Semiconductor Laser Conference, the 2001 International Conference on Modulated Semiconductor Structures, the 2002 International Conference on Quantum Dots, and the 2005 International Quantum Electronics Conference. He was the recipient of the IBM Science Award, the Hattori Hoko Award, the Nissan Science Award, the ISCS Quantum Device Award, the IEEE William Streifer Award, and the Leo Esaki Prize. He is the Editor-in-Chief of *Solid State Electronics*.